

OPEN ACCESS

Differential inertial focusing of particles in curved low-aspect-ratio microchannels

To cite this article: Aman Russom *et al* 2009 *New J. Phys.* **11** 075025

View the [article online](#) for updates and enhancements.

You may also like

- [Condensate deformation and quantum depletion of Bose–Einstein condensates in external potentials](#)
C A Müller and C Gaul
- [Tunable hyperbolic out-of-plane deformation of 3D-printed auxetic PLA shape memory arrays](#)
Zhenghong Li, Yuheng Liu, Haibao Lu et al.
- [Fast growing resistive two fluid instabilities in hybrid-like tokamak configuration](#)
D Brunetti, J P Graves, W A Cooper et al.

Differential inertial focusing of particles in curved low-aspect-ratio microchannels

Aman Russom¹, Amit K Gupta, Sunitha Nagrath, Dino Di Carlo, Jon F Edd and Mehmet Toner

BioMEMS Resource Center, Center for Engineering in Medicine and Surgical Services, Massachusetts General Hospital, Shriners Hospital for Children, and Harvard Medical School, Boston, MA 02114, USA

E-mail: aman@kth.se

New Journal of Physics **11** (2009) 075025 (9pp)

Received 3 February 2009

Published 31 July 2009

Online at <http://www.njp.org/>

doi:10.1088/1367-2630/11/7/075025

Abstract. Microfluidic-based manipulation of particles is of great interest due to the insight it provides into the physics of hydrodynamic forces. Here, we study a particle-size-dependent phenomenon based on differential inertial focusing that utilizes the flow characteristics of curved, low aspect ratio (channel width \gg height), microfluidic channels. We report the emergence of two focusing points along the height of the channel (z -plane), where different sized particles are focused and ordered in evenly spaced trains at correspondingly different lateral positions within the channel cross-section. We applied the system for continuous ordering and separation of suspension particles.

Contents

1. Introduction	2
2. Particle focusing	2
3. Differential focusing domain	5
4. Application: high throughput separation	7
5. Conclusions	8
Acknowledgments	9
Reference	9

¹ Author to whom any correspondence should be addressed.

1. Introduction

Separation of suspended micrometer-sized or smaller particles is of fundamental importance in the biological and biomedical field. In recent years, microfluidic particle separation systems have emerged as attractive alternatives to conventional techniques. Separation based on externally applied forces, such as dielectrophoresis [1, 2], magnetophoresis [3], acoustic waves [4] and optical interference patterns [5] have been described on the microscale. Other methods achieve separation by filtering of particles through sieving structures [6]–[8] or by differential interaction of particles with local flow profiles [9]–[13]. Unfortunately, most of these systems have an inherent limitation as the operating flow rates are too low for high throughput applications. Here, we report differential inertial focusing to continuously separate particles at throughput comparable to macroscale systems.

Lateral migration due to inertial lift forces was first experimentally shown by Segré and Silberberg where they observed that particles in a cylindrical Poiseuille flow (pipe of radius R) migrated to an equilibrium position located at $r = 0.62R$ for small Reynolds number (Re) [14]. Their work triggered a series of experimental and theoretical studies. Karnis *et al* [15] observed that particles stabilize midway between the centerline and the wall, closer to the wall for larger flow rates and closer to the center for larger particles due to the inertia effect of the flow. Tachibana [16] found experimentally that the lateral migration of spheres in pipe flows depends mainly on the ratio of the sphere diameter to the pipe diameter and that the phenomenon is clearly observed if this ratio exceeds about 0.2. When Re is increased, the Segré–Silberberg equilibrium position moves toward the wall [17, 18], in agreement with theoretical predictions [19, 20]. In a similar pipe flow system, Matas *et al* [21] observed trains of particles aligned with the flow located in the Segré–Silberberg equilibrium position. Recently, lateral particle migration was extended by our group to rectangular microfluidic channels where focusing of microparticles could be observed in four positions [22]. Reducing the symmetry of rectangular channels by introducing repetitive curvatures enabled the focus positions of particles to be reduced to a single stream [22]. The addition of curvature introduces a secondary cross-sectional flow field perpendicular to the flow direction (Dean flow) [23]. Notably, particles in a curvilinear channel can follow secondary vortices causing them to migrate across the main streamlines in the direction of flow. Separation and filtration according to size were recently demonstrated for particles flowing through curved channels [24]–[26].

In this work, particle flow through curved, low-aspect-ratio (width \gg height), microchannels is examined for non-small particles. We communicate novel findings for flows through spiral microchannels with requisite geometrical features resulting in particle focusing and ordering. We report particle focusing in two distinct focusing points along the height of the channel (z -plane), and show here for the first time that particles focus to different parallel streamlines within the transverse plane of the channel depending on the particle size. Finally, we utilize the focusing phenomenon for continuous, high throughput, particle separation.

2. Particle focusing

Lateral migration of particles in parabolic shear flow arises from dominant lift forces (F_L) due to the presence of a shear-gradient-induced inertia that is directed down the shear gradient toward the wall and the wall-induced inertia that pushes particles away from the stationary wall [20]. For a low-aspect-ratio (width \gg height) rectangular geometry, the lift force along the

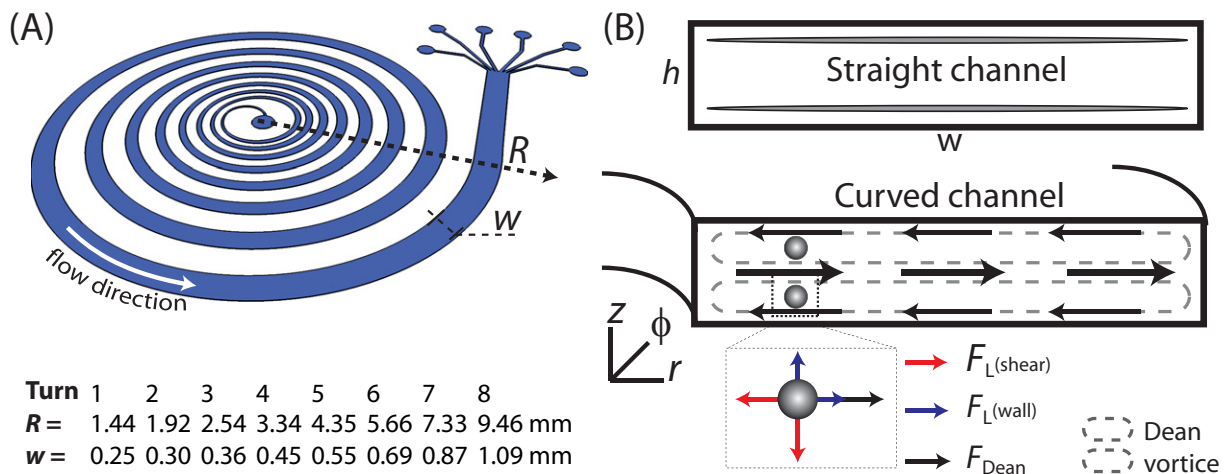


Figure 1. (A) The spiral device, produced in PDMS using standard lithography technique, consists of 8 turns with channel width increasing with the radius of curvature and a total footprint of 2.1 cm in diameter. (B) Schematic illustration of particle focusing points along the height of the channel (z -plane) for straight rectangular (top) and curved (bottom) channels. Dominant forces acting on a particle focused in a distinct point along the height of the curved channel are highlighted.

dimension defined by the channel height is dominant and it is expected that particles will tend to focus into two laterally broad focusing positions (top and bottom of the rectangular channel, see figure 1(B) upper panel), which is consistent with previous observations [27, 28].

As stated above, adding curvature introduces a secondary rotational flow-field perpendicular to the flow direction (Dean flow). This flow is characterized by the presence of two counter-rotating vortices, located above and below the plane of symmetry of the channel [18, 22] (figure 1(B), lower panel). The transverse Dean flow introduces a drag force (F_D) that moves particles at the top and bottom laterally toward the inner wall; however, if they are closer to the mid-plane in the z -direction, the particles are pushed toward the outer wall and recirculated following the top or bottom stream lines allowing them to quickly find their lateral equilibrium positions.

F_L and F_D vary in magnitude across the channel cross section and the functional form of this variation is currently not known. However, two dimensionless numbers, particle Reynolds number (R_p) and Dean number (De), can be used to explain how these forces scale in flows through curved channels. R_p [$= Re(a/D_h)^2$] depends on the intrinsic properties of the fluid, described by the channel Reynolds number, Re [$= \rho U_m D_h / \mu$]; particle diameter (a) and channel dimension (D_h). D_h is the hydraulic diameter (defined as $D_h = 2wh / (w + h)$, where w and h are the width and height of the channel). U_m is the maximum channel velocity; μ and ρ are the viscosity and density of the fluid, respectively. Dean number, De [$= Re(D_h/2r)^{1/2}$], is a measure of the magnitude of the secondary flow (Dean flow) due to curvature; where r is the radius of the curvature. F_L has been shown to scale with the particle Reynolds number squared (R_p^2) and a lift coefficient (f_c) [$F_L = R_p^2 f_c \mu^2 / \rho$] [20]. F_D scales with the downstream velocity squared (U_m^2) [$F_D \sim \rho U_m^2 a D_h^2 / r$] [29]. To harness the interplay between these two

dominant forces, we designed and evaluated a microfluidic spiral device with low-aspect-ratio (width \gg height) rectangular cross-section geometry and channel width that increases with the radius of curvature according to figure 1(A). The device, with a footprint diameter of 2.1 cm and consisting of 8 turns, was fabricated by casting polydimethylsiloxane (PDMS) according to standard soft lithographic techniques and was bonded to a glass slide. Figure 1(B) shows a schematic illustration of how the two dominant forces, F_L and F_D , can interplay to trap particles flowing through a curved channel at an equilibrium position. Depending on the relative magnitude of the F_D and F_L acting on a particle, focusing (dominant lift) or mixing (dominant Dean flow) can occur.

The experimental systems consist of analyzing microparticles flowing through the spiral channel. We found strong R_p ($\propto (a/D_h)^2$) dependence for particle focusing. Figure 2(A) shows result of fluorescent polystyrene (density $\sim 1.05 \text{ g ml}^{-1}$) particles 10 and $2 \mu\text{m}$ in diameter suspended in water (density $\sim 1.0 \text{ g ml}^{-1}$) flown through a $50 \mu\text{m}$ -high spiral channel at a volumetric flow rate of 2 ml min^{-1} ($Re = 166$ at turn 5, with corresponding $R_p(10 \mu\text{m}) = 2$ and $R_p(2 \mu\text{m}) = 0.08$). The $10 \mu\text{m}$ particles, initially well distributed at the inlet, quickly focus while the $2 \mu\text{m}$ particles remained unfocused, indicating R_p dependence for focusing (figure 2(A)). Figure 2(B) shows a high-speed image at the outlet (turn 8, $R_p(10 \mu\text{m}) = 1$ and $R_p(2 \mu\text{m}) = 0.04$), where the larger $10 \mu\text{m}$ particles are kept focused in a single lateral stream while the $2 \mu\text{m}$ particles are pushed away from the inner wall and scattered across the channel. In addition to focusing, particles are ordered in regular, evenly spaced, longitudinal trains focused in two parallel streams along the height of the channel (figure 2(C)). These ordered particles often alternate in the z -plane and maintain uniform longitudinal spacing due to particle–particle interactions within and across the two z -plane streamlines, in agreement with previous observations for flows through straight, high aspect ratio, channels [27].

F_L and F_D vary in magnitude across the channel cross section and the functional form of this variation is currently not known. In an effort to gain insight into the underlying mechanism of focusing phenomena, in particular additional radial forces of a magnitude that can compete with the inertial lift force, we evaluated the influence of centrifugal force ($F_{\text{cfg}} = \rho_p(\pi/6)a^3(U_p^2/r)r'$) on particle focusing. Here, ρ_p , U_p and r are particle density, downstream velocity and the radius at which a particle is focused. We calculated F_{cfg} for two representative cases at which $10 \mu\text{m}$ particles are focused (spiral turn 5 for $R_p = 0.5$ and turn 6 for $R_p = 0.8$). F_{cfg} was 5 pN in both cases, which is an order of magnitude smaller than the expected Dean force. We obtained the lateral positions for particles (r) from experimental observations and the downstream velocity (U_p) from high-speed camera measurements. It should be noted that centrifugal forces are even less important with smaller particles ($F_{\text{cfg}} \propto a^3$ while $F_D \propto a$).

At average flow rates at which the particle focusing occurs, sedimentation velocities are orders of magnitude lower than the translational velocities in the direction of the flow and particle sedimentation due to buoyancy may be neglected. Experimentally, we tested density independence and found particles (polystyrene, density $\sim 1.05 \text{ g ml}^{-1}$) suspended in solutions of both higher (CaCl_2 solution of density $\sim 1.2 \text{ g ml}^{-1}$) and lower density (water, density $\sim 1.0 \text{ g ml}^{-1}$) were successfully focused. In addition, we found no notable difference in focusing position for $10 \mu\text{m}$ polystyrene particles and silica particles (density $\sim 2 \text{ g ml}^{-1}$) suspended in water. These findings suggest that focusing is largely independent of centrifugal forces acting on particles. Based on this preliminary analysis, it appears that Dean drag is the dominant lateral force to balance the influence of lift forces acting on particles.

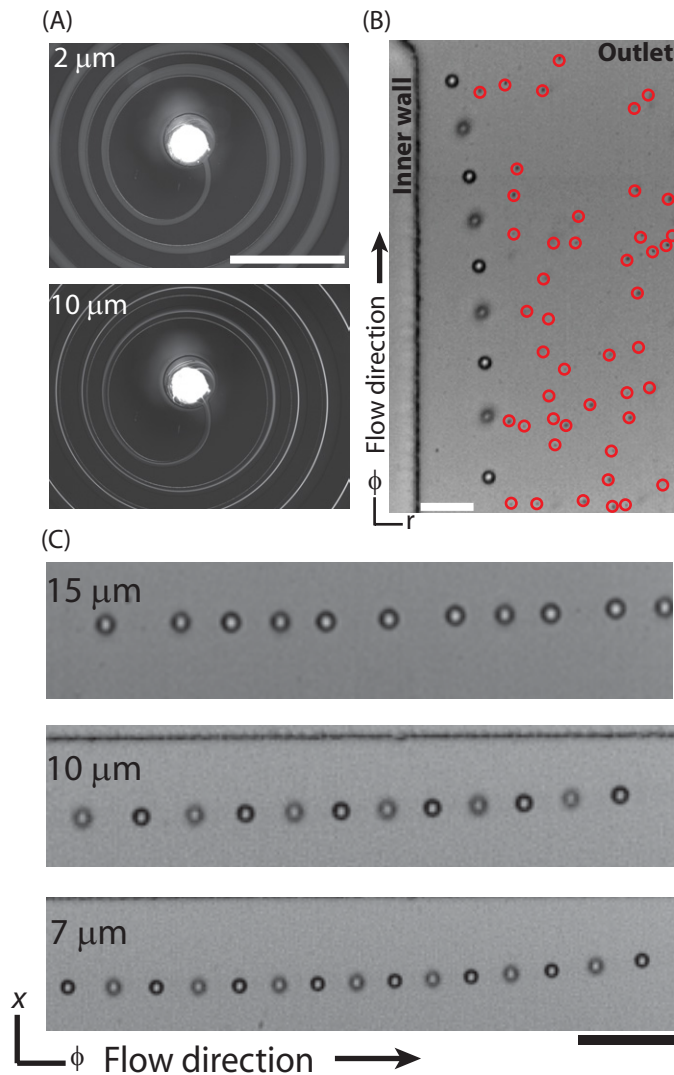


Figure 2. Particle focusing and ordering in a microfluidic spiral device. (A) Fluorescence image of a particle mixture ($2\ \mu\text{m}$, green and $10\ \mu\text{m}$, red) flowing together through a device at a flow rate of $2\ \text{ml min}^{-1}$ ($Re = 166$ at turn 5 of the spiral). Scale bar: $2\ \text{mm}$. (B) Image at the outlet (flow rate of $2\ \text{ml min}^{-1}$, $Re = 88$) showing self-ordered, longitudinally alternate positioned particle trains of $10\ \mu\text{m}$ particles. The scattered $2\ \mu\text{m}$ particles are highlighted for clarity. Scale bar: $50\ \mu\text{m}$. (C) Alternating particle trains of three different particle sizes flowing at $2\ \text{ml min}^{-1}$. Scale bar: $50\ \mu\text{m}$.

3. Differential focusing domain

For a low-aspect-ratio channel geometry, the height is the dominant factor and the hydraulic diameter can be expressed as $D_h = 2h$, and focusing is therefore strongly dependent on the a/h ratio ($R_p \propto (a/h)^2$). In figure 3, experimental a/h ratio values are plotted against De for a range of particle diameters and channel geometries. Experimentally, we measured the width

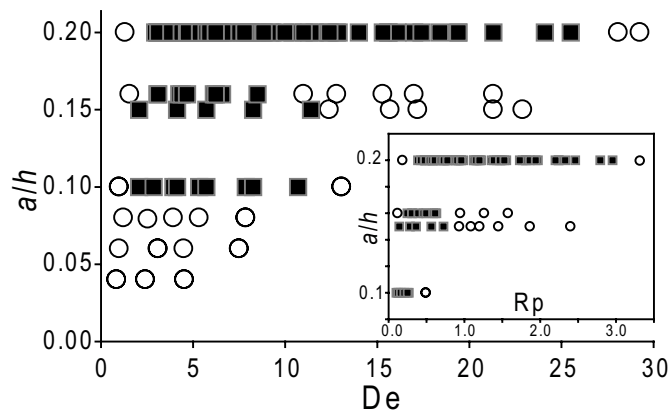


Figure 3. Particle focusing behavior. Graph of particle size to channel height (a/h) ratio plotted against the Dean number (De). Each point: (■) for focused and (○) for unfocused particles, represent data generated from turn 5 to 8 of the spiral device. A minimum a/h ratio > 0.1 is required for focusing. Inset shows the corresponding graph for a/h against particle Reynolds number (R_p) for the ratios that generate focusing.

and shape of the fluorescent intensity and defined the cut-off for single stream focusing if the half-intensity-width is less than $3a$. Three regimes can be distinguished from figure 3: at low De (regime 1), all particles remained unfocused, presumably due to insufficient lift and Dean forces. At intermediate De (regime 2), focusing is observed due to lift dominating over Dean forces ($F_L > F_D$). Our results suggest a minimum a/h ratio > 0.1 for focusing. At high De (regime 3), the particles start to defocus from a single stream to multiple streams as F_D starts to dominate over F_L . As indicated by figure 3 (inset), the higher the a/h ratio, the higher the velocity that can be maintained without defocusing. Our findings suggest focusing is primarily dictated by the lift forces ($\propto R_p^2$), while Dean forces may initially act to ‘speed up’ the focusing by acting on particles to quickly find their lateral equilibrium position. With increased velocity, F_D increases faster than F_L [22] leading to shift in dominance ($F_L < F_D$) and defocusing behavior is observed.

Effective separation of focused particles can be achieved in low-aspect-ratio geometries, where a small change in particle size will affect the balance between the lift and Dean forces which, when combined with variation of these forces across the channel face, leads to focusing of different sized particles in different streams in the radial direction. Figure 4(A) shows $10 \mu\text{m}$ particles, initially focused close to the inner wall, progressively displaced away from the inner wall without defocusing with increasing fluid velocity. This suggests that precise control of the lateral position can be achieved by varying the flow rate for a given channel geometry. The unique feature of the spiral device with increasing channel width with radius of curvature results in decreased Re due to increased cross-section area. This allows very high flow rates while maintaining single stream focusing and a relatively small lateral displacement from the inner wall with increased spiral turns. Furthermore, to test focusing of different particle sizes to different parallel streams concurrently, 10 and $7 \mu\text{m}$ particles were mixed and flowed through the system together. At low Re , both particle sizes are displaced to overlapping streams. As Re increases both particle sizes are laterally displaced away from the inner wall.

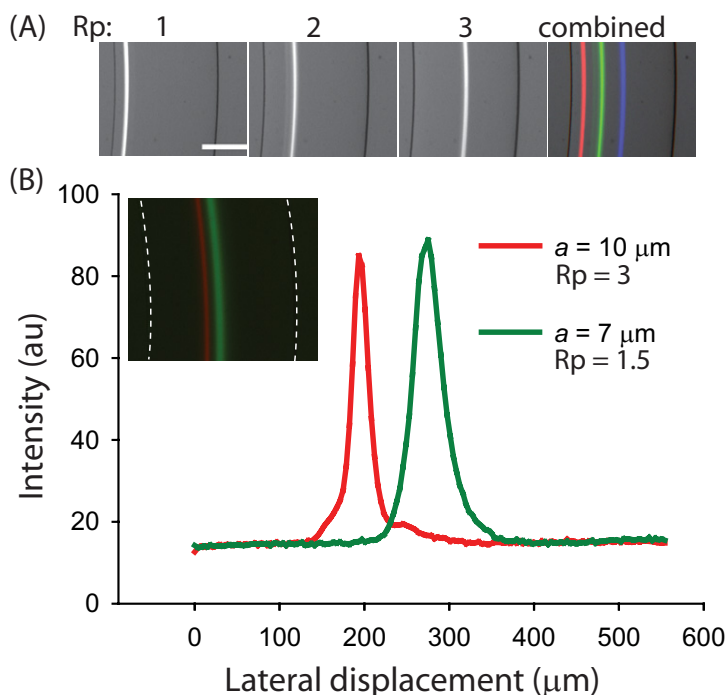


Figure 4. Control of lateral position for differential displacement. (A) Lateral displacement of $10 \mu\text{m}$ particles flowing through a $50 \mu\text{m}$ high channel as a function of R_p at spiral turn 5. The right panel illustrates superimposed figures of the three different flow conditions ($R_p = 1; 2; 3$). Scale bar: $145 \mu\text{m}$. (B) Intensity cross section of differentially focused 10 and $7 \mu\text{m}$ particles flowing together at $Re = 252$ (corresponding to $R_p = 3$ and 1.5). The particles are clearly separated into different parallel streams. Inset shows the intensity of $10 \mu\text{m}$ (red) and $7 \mu\text{m}$ (green) particles from which the cross-section intensity was obtained. The walls are highlighted with dotted lines for clarity.

However, the smaller $7 \mu\text{m}$ particles drift further away from the inner wall when compared with the $10 \mu\text{m}$ particles (figure 4(B)). The $10 \mu\text{m}$ ($R_p = 3$) and $7 \mu\text{m}$ ($R_p = 1.5$) particles are completely separated into two parallel streams 193 and $275 \mu\text{m}$ away from the inner wall for the respective sizes. Hence, the system can enable continuous separation between two or more differentially focused particles, a new important enabling capability for inertial-induced sorting. The possibility to control the position of particles in continuously flowing microfluidic channels at very high throughput opens the door to the development of a whole set of bioanalytical applications.

4. Application: high throughput separation

Sorting and separation of microparticles and biological cells plays a major role in many chemical and biological processes. To evaluate the system for separation, we fabricated a device with two outlets, a $50 \mu\text{m}$ wide (outlet 1) channel at the inner wall and $950 \mu\text{m}$ wide channel (outlet 2). A mixture of 10 and $3 \mu\text{m}$ particles was pushed through a device $50 \mu\text{m}$ in height at a flow rate of 3.5 ml min^{-1} (with corresponding $Re = 153$ at turn 8 of the device) to evaluate the

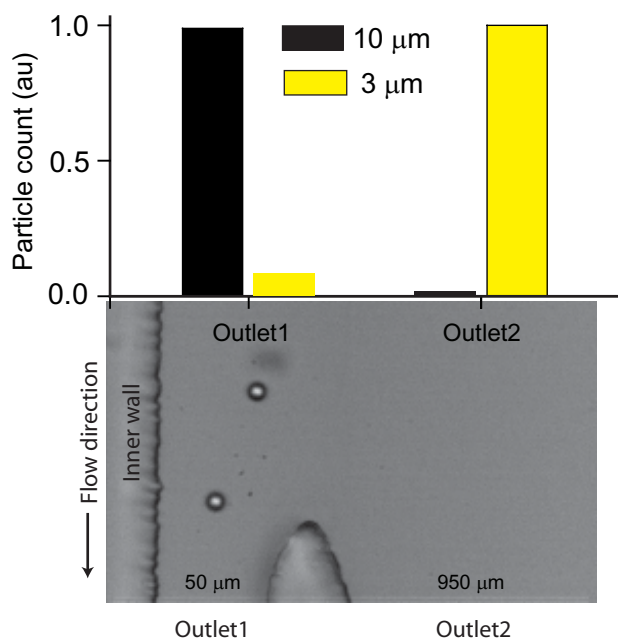


Figure 5. High throughput separation. (Upper) Coulter counter results of 10 and 3 μm particle mixture flowed through a device, 50 μm in height, and collected from outlets 1 and 2. (Lower) High-speed image at the outlets, clearly showing ordered 10 μm particles flowing to outlet 1.

separation efficiency. The 10 μm particles were focused close to the inner wall and successfully recovered through outlet 1, while the 3 μm particles remained unfocused and pushed away from the inner wall and could be collected at outlet 2. A Coulter counter was used to count the two fractions (figure 5). The yield of the 10 μm particles, calculated as fraction of 10 μm particles recovered through outlet 1 to the total count, was 98.5%, and the yield was 92.5% for 3 μm particles in outlet 2. A good measure of the separation efficiency for a system is to evaluate the enrichment ratio, a measure that takes the initial particle concentrations into account and is defined as the number of selected particles (s_f) to unselected particles (u_f) in the fraction (outlet 1 for 10 μm particles and outlet 2 for 3 μm particles) divided by the initial fraction of selected (s_i) to unselected particles (u_i) (enrichment ratio = $s_f/u_f/s_i/u_i = (s_f u_i)/(s_i u_f)$) in the inlet. Thus, enrichment is dependent on depleting the unselected particles but also on maintaining high yields of the selected particles (s_f/s_i). In our system, an enrichment ratio of 64 was achieved for the 3 μm particles and 13 for the 10 μm particles. The high enrichment ratio indicates very efficient separation of particles. To reiterate, the volumetric flow rate used was 3.5 ml min^{-1} , a throughput comparable to macroscale systems.

5. Conclusions

In summary, we report flows through curved channels with rectangular low-aspect-ratio cross-section geometries and describe how the combined effect of lift and Dean forces can interplay to focus and order particle suspensions. We provide data suggesting that particles are focused in two symmetrical positions along the height of the channel. Specifically, using the critical nature

of the particle size with respect to channel dimensions and the defined flow parameters, we were able to differentially focus particles of various sizes into evenly spaced train formations at different lateral positions within the channel cross-section. This simple continuous particle processing method does not require external forces to operate and should be readily applicable to complex separation tasks.

Acknowledgments

This work was supported by the National Institute of Health (P41 EB-002503). Octavio Hurtado is acknowledged for help with microfabrication and we thank Ramin Haghgoie for discussions.

Reference

- [1] Kang K H *et al* 2006 *Electrophoresis* **27** 694
- [2] Chen D F, Du H and Li W H 2006 *J. Micromech. Microeng.* **16** 1162
- [3] Pamme N and Manz A 2004 *Anal. Chem.* **76** 7250
- [4] Petersson F *et al* 2005 *Anal. Chem.* **77** 1216
- [5] MacDonald M P, Spalding G C and Dholakia K 2006 *Nature* **426** 421
- [6] Zhu L *et al* 2004 *Lab Chip* **4** 337
- [7] Sethu P, Sin A and Toner M 2006 *Lab Chip* **6** 83
- [8] Chen *et al* 2006 *Surf. Interface Anal.* **38** 996
- [9] Yamada M, Nakashima M and Seki M 2004 *Anal. Chem.* **76** 5465
- [10] Yamada M and Seki M 2006 *Anal. Chem.* **78** 1357
- [11] Yang S, Undar A and Zahn J D 2006 *Lab Chip* **6** 871
- [12] Zhang X *et al* 2006 *Lab Chip* **6** 561
- [13] Huang L R *et al* 2004 *Science* **304** 987
- [14] Segre G and Silberberg A 1961 *Nature* **189**
- [15] Karnis A, Goldsmith H L and Mason S G 1966 *Can. J. Chem. Eng.* **44** 181
- [16] Tachibana M 1973 *Rheol. Acta* **12** 58
- [17] Segre G and Silberberg A 1962 *J. Fluid Mech.* **14** 136
- [18] Matas J P, Morris J F and Guazzelli E 2004 *Oil Gas Sci. Technol.* **59** 59
- [19] Schonberg J A and Hinch E J 1989 *J. Fluid Mech.* **203** 517
- [20] Asmolov E S 1999 *J. Fluid Mech.* **381** 63
- [21] Matas J, Glezer V and Guazzelli E 2004 *Phys. Fluids* **16** 5
- [22] Di Carlo D *et al* 2007 *Proc. Natl Acad. Sci. USA* **104** 18892
- [23] Dean W 1928 *Phil. Mag.* **5** 22
- [24] Di Carlo D *et al* 2008 *Anal. Chem.* **80** 2204
- [25] Seo J, Lean M H and Kole A 2007 *J. Chromatogr.* **1162** 126
- [26] Bhagat A, Kuntaegowdanahalli S and Papautsky I 2008 *Lab Chip* **8** 1906
- [27] Edd J F *et al* 2008 *Lab Chip* **8** 1262
- [28] Bhagat A A S, Kuntaegowdanahalli S S and Papautsky I 2008 *Phys. Fluids* **20** 101702
- [29] Squires T M and Quake S R 2005 *Rev. Mod. Phys.* **77** 50